Signal Processing 140 (2017) 190–197

Contents lists available at ScienceDirect

Signal Processing

journal homepage: www.elsevier.com/locate/sigpro

Robust minimum dispersion distortionless response beamforming against fast-moving interferences

Liang Zhang[a], Bo Li[b], Lei Huang[a,*], Thiagalingam Kirubarajan[b], Hing Cheung So[c]

[a] College of Information Engineering, Shenzhen University, Shenzhen, PR China
[b] Department of Electrical and Computer Engineering, McMaster University, Hamilton, Canada
[c] Department of Electronic Engineering, City University of Hong Kong, Hong Kong

ARTICLE INFO

Article history:
Received 4 January 2017
Revised 30 March 2017
Accepted 27 April 2017
Available online 12 May 2017

MSC:
00-01
99-00

Keywords:
Beamforming
Interference suppression
Minimum dispersion
Sub-Gaussian signals
Fast-moving interferences

ABSTRACT

The recently proposed minimum dispersion distortionless response (MDDR) beamformer is able to improve the reception of non-Gaussian signals over the minimum variance distortionless response (MVDR) beamformer. However, the performance of the MDDR beamformer degrades in the presence of fast-moving interferences. To suppress such an interference, a robust beamformer against fast-moving interferences based on the minimum dispersion (MD) criterion is proposed, which provides a continuous deep null sector over a predefined range of dynamic angle-of-arrival (AOA). The designed beamformer ensures that the output is minimized in terms of dispersion and the average power over the dynamic AOA is zero via a quadratic constraint. In order to reduce the computational load, the optimization problem with a quadratic constraint is relaxed to its counterpart with a linear constraint. This allows us to devise an efficient beamforming approach, namely, gradient projection algorithm. Numerical results are provided to demonstrate that the developed beamformer can suppress the strong fast-moving interferences effectively.

1. Introduction

Beamforming is a spatial filter used to enhance the signal-of-interest (SOI) and mitigate the interference as well as noise. It has been widely used in radar, sonar, communications, biomedical and audio signal processing [1–4].

Compared with conventional delay-and-sum beamforming, adaptive beamforming approaches are able to more efficiently enhance the SOI and suppress interference and noise [1]. However, the performances of most adaptive beamforming techniques deteriorate under challenging environments such as angle-of-arrival (AOA) mismatch, imperfect array calibration, and sensor location error. In order to tackle this issue of robust beamforming in some challenging scenarios, various adaptive beamforming algorithms under the minimum variance (MV) criterion have been suggested [1,5–12]. In this work, we consider two commonly encountered situations where the performances of adaptive beamforming algorithms degrade.

In the first case, a fast-moving interference crosses the observation region of a receiving array, in which the AOA of the interference is not fixed but varies with time. Such an interference will influence the SOI reception and results in reduction of output signal-to-interference-plus-noise ratio (SINR). Usually, a null is designed to cancel the interference by making the response to the interference with zero [13]. With multiple interferences, multiple similar constraints are imposed, which lead to the linearly constrained minimum variance (LCMV) beamformer [4]. However, in this case, the degree-of-freedom of the LCMV beamformer is affected to the number of linear constraints. The LCMV beamformer does not perform well with an interference whose AOA varies quickly with time. Unlike the LCMV approach, the null-broadening technique provides a null sector to suppress a fast-moving interference. In [14], the interferers were made to cover a greater angular extent by applying a transformation to the sample covariance matrix (SCM). As the transformation in [14] would introduce the noise contribution to the SCM, the method of dispersion synthesis was proposed in [15] to avoid additional noise power involved in the SCM. In [15], adaptive trough patterns were produced by distributing a cluster of virtual equal-strength incoherent interferences around each original source. The null-broadening method of derivative constraint was proposed in [16,17], but has a much greater computational load than those of [14,15]. The minimum power distortionless response (MPDR) beamformer, which constrained the output power in a predefined angular sector below a pre-specified suppression level by using a quadratic con-

* Corresponding author.
E-mail address: lhuang@szu.edu.cn (L. Huang).

http://dx.doi.org/10.1016/j.sigpro.2017.04.019
0165-1684/

straint, was proposed in [18]. To reduce computational complexity, the original quadratic constraint in [18] was replaced with a set of linear constraints in [19] to produce a widened null sector over the fast-moving interference.

In the second case, the signals and interferences encountered in practice are often non-Gaussian distributed. Zero-mean random signals can be classified as super-Gaussian, Gaussian and sub-Gaussian, according to the kurtosis measure which describes the tail shapes of their distributions [20]. Most of the encountered signals in practice are non-Gaussian distributed, e.g., speech, acoustic signals, and modulated signals in radar, sonar, GPS navigation and wireless communications [21]. The beamformers based on the MV criterion are optimal for Gaussian signals, because they make full use of the second-order statistical information of Gaussian signals. For non-Gaussian situations, however, the MV beamformer suffers performance degradation as the higher-order and lower-order statistical information has been ignored. The non-Gaussianity of signals applied to blind beamforming and impulsive noise suppression were considered in [22,23]. The minimum dispersion distortionless response (MDDR) beamformer for non-Gaussian signals, which minimizes the ℓ_p-norm of the output while constraining the response of SOI to unity, was proposed in [24–27]. The MDDR beamformer exhibits better performance of non-Gaussian signals reception than the minimum variance distortionless response (MVDR) beamformer.

Although the MDDR beamformer exhibits superior performance for non-Gaussian signal reception, its performance deteriorates in the presence of fast-moving interferences. To tackle this issue, we devise a new beamforming approach based on the minimum dispersion (MD) criterion [24], which is able to eliminate the power of the interference from the beamformer output by constraining the average power of the interference's dynamic angular sector to zero. This provides a broad deep null sector, which in turn enables us to handle the fast-moving interferences. The proposed beamformer has two advantages: First, it shares the same performance with the MDDR beamformer for sub-Gaussian signal reception; Second, it is much more robust against fast-moving interferences than the MVDR and MDDR beamformers.

Moreover, the optimization problem in the proposed beamformer consists of a convex objective function and a linear constraint. This problem can be solved using the software of interior-point method (IPM) via CVX and SeDuMi [28]. In order to reduce the computational load, the gradient projection (GP) algorithm is applied to solve the optimization problem. Besides, the computational complexity of the algorithm is also analysed.

This paper is organized as follows: Section 2 presents the signal model for array processing along with a brief introduction to the MPDR and standard MDDR beamformers. In Section 3, the linearly constrained MDDR beamforming approach is formulated in the case of fast-moving interferences. To solve the linearly constrained optimization problem for MDDR beamformer, the GP algorithm is revisited. Computer simulations are performed to evaluate the performance of the proposed beamformer in Section 4. Finally, conclusions are drawn in Section 5.

2. Background

2.1. Signal model

Consider a uniform linear array (ULA) with M omnidirectional receiving sensors. Assume that P uncorrelated narrowband signals s_i $(i = 0, 1, \cdots, P-1)$ impinge on the array with AOAs θ_i $(i = 0, 1, \cdots, P-1)$, where s_0 is the SOI. The signal received by the array at the nth time instant is mathematically expressed as

$$\boldsymbol{x}(n) = \boldsymbol{\alpha}(\theta_0)s_0(n) + \sum_{i=1}^{P-1}\boldsymbol{\alpha}(\theta_i)s_i(n) + \boldsymbol{e}(n), \tag{1}$$

where $\{\boldsymbol{\alpha}(\theta_i)\}_{i=0}^{P-1}$ are the steering vectors of the SOI and interferences, and $\boldsymbol{e}(n)$ is the additive noise. The steering vector $\boldsymbol{\alpha}(\theta)$ is given by

$$\boldsymbol{\alpha}(\theta) = \left[1, e^{j(2\pi/\zeta)d\sin(\theta)}, \cdots, e^{j(M-1)(2\pi/\zeta)d\sin(\theta)}\right]^T, \tag{2}$$

where ζ is the wavelength, d is the inter-element spacing, and $(\cdot)^T$ represents the transpose operator.

In order to enhance the reception of SOI and mitigate the interference as well as noise, the beamforming weight vector is designed following a certainty criterion, which is recorded as $\boldsymbol{w} \in \mathbb{C}^M$. Therefore, the beamformer output can be expressed as

$$y(n) = \boldsymbol{w}^H\boldsymbol{x}(n), \tag{3}$$

where $(\cdot)^H$ denotes the Hermitian transpose. The beamformer output SINR is defined as

$$\mathrm{SINR} \triangleq \frac{\mathrm{E}\{|\boldsymbol{w}^H\boldsymbol{\alpha}(\theta_0)s_0(n)|^2\}}{\mathrm{E}\{|\boldsymbol{w}^H(\boldsymbol{i}(n)+\boldsymbol{e}(n))|^2\}} = \frac{\sigma_s^2|\boldsymbol{w}^H\boldsymbol{\alpha}(\theta_0)|^2}{\boldsymbol{w}^H\boldsymbol{R}_{i+n}\boldsymbol{w}}, \tag{4}$$

where $\boldsymbol{i}(n)$ is the interference impinging on the array defined as $\boldsymbol{i}(n) = \sum_{i=1}^{P-1}\boldsymbol{\alpha}(\theta_i)s_i(n)$, $\sigma_s^2 = \mathrm{E}\{|s_0(n)|^2\}$ is the variance of the SOI, $\boldsymbol{R}_{i+n}$ is the interference-plus-noise covariance matrix, and $\mathrm{E}\{\cdot\}$ denotes the expectation operator.

2.2. MPDR Beamformer

Consider the commonly encountered scenario in practice that a fast-moving interference crosses the observation region, where the AOA of the interference varies with time. In this situation, an interference can be anywhere in $[\theta_{\min}, \theta_{\max}]$, which poses a big challenge for accurate reception of the SOI and effective suppression of interference. The MPDR beamformer [19], which designs a broad null sector over $[\theta_{\min}, \theta_{\max}]$ with a pre-specified suppression level, is reformulated in this work to handle the issue of robust beamforming against fast-moving interferences. It can be expressed as the following constrained optimization problem:

$$\begin{aligned} \min_{\boldsymbol{w}} \quad & \boldsymbol{w}^H\boldsymbol{R}_{i+n}\boldsymbol{w} \\ \text{s.t.} \quad & \boldsymbol{w}^H\boldsymbol{\alpha}(\theta_0) = 1 \\ & \boldsymbol{w}^H\boldsymbol{Q}\boldsymbol{w} \le \eta, \end{aligned} \tag{5}$$

where $\boldsymbol{Q} = 1/(\theta_{\max}-\theta_{\min})\int_{\theta_{\min}}^{\theta_{\max}}\boldsymbol{\alpha}(\theta)\boldsymbol{\alpha}^H(\theta)d\theta$, and η denotes the pre-specified level of the broad null sector. The solution of (5) minimizes the beamformer output, not only subject to a distortionless constraint but also subject to a constraint that the average power over $[\theta_{\min}, \theta_{\max}]$ is under a pre-specified level η.

2.3. Standard MDDR beamformer

A random signal $s(n)$ with zero-mean can be classified according to its kurtosis, which is defined as

$$\kappa_s = \frac{\mathrm{E}\left\{|s(n)|^4\right\}}{\sigma_s^4}. \tag{6}$$

Here, $s(n)$ belongs to the class of sub-Gaussian signals if $\kappa_s < 3$; $s(n)$ is a super-Gaussian signal if $\kappa_s > 3$; and the kurtosis of a Gaussian signal is equal to 3. Super-Gaussian signals are very common in practice, such as speech, biomedical signals and impulsive noise [20,29,30]. Sub-Gaussian signals are widely used in sonar, radar and GPS navigation, such as quadrature phase-shift keying

(QPSK), quadrature amplitude modulation (QAM) and other communication signals [20,21].

The MDDR beamformer is proposed for non-Gaussian signals by exploiting the ℓ_p-norm of the data received by the array. Specifically, the corresponding optimization problem is formulated as

$$\begin{aligned} \min_{\boldsymbol{w}} \quad & \mathrm{E}\left\{\left|\boldsymbol{w}^H\boldsymbol{x}(n)\right|^p\right\} \\ \text{s.t.} \quad & \boldsymbol{w}^H\boldsymbol{\alpha}(\theta_0)=1. \end{aligned} \tag{7}$$

Since $\mathrm{E}\{|\cdot|^p\}$ is referred to as the dispersion of a random variable in statistics, which is also the generalization of variance for non-Gaussian signals, the MVDR beamformer is a special case of the MDDR beamformer when $p=2$.

3. Linearly constrained minimum dispersion beamforming against fast-moving interference

3.1. Robust MDDR beamformer against fast-moving interference

The standard MDDR beamformer exhibits excellent performance for non-Gaussian signal reception. However, it deteriorates in the presence of a fast-moving interference. To suppress such an interference, a robust beamformer based on the MD criterion is proposed in this section, which provides a continuous deep null sector over a predefined range of dynamic AOA.

3.1.1. Linearly constrained MDDR beamformer

As the fast-moving interferences usually exhibit the property of sub-Gaussian distribution [20,21], this paper just focuses on the sub-Gaussian scenarios. Therefore, unless stated otherwise the signals and interferences are assumed to be sub-Gaussian and $p>2$ is adopted, while the additive noise is Gaussian distributed.

Due to finite samples, replacing the expectation with the sample mean and discarding the constant $1/N$, (7) is rewritten as

$$\begin{aligned} \min_{\boldsymbol{w}} \quad & F(\boldsymbol{w})=\left\|\boldsymbol{X}^H\boldsymbol{w}\right\|_p^p \qquad (p>2) \\ \text{s.t.} \quad & \boldsymbol{w}^H\boldsymbol{\alpha}(\theta_0)=1, \end{aligned} \tag{8}$$

where $\boldsymbol{X}=[\boldsymbol{x}(1),\cdots,\boldsymbol{x}(N)]$ contains the data received by the array, with the number of snapshots being N, and $\boldsymbol{x}(n)\in\mathbb{C}^M$ for $n=1,\cdots,N$.

Motivated by the MPDR beamformer described in Section 2.2, the fast-moving interference can be suppressed by eliminating the average power over the sector $[\theta_{I,0}-\triangle\theta,\theta_{I,0}+\triangle\theta]$ from the MDDR beamformer output. Therefore, the MDDR beamformer with a broad null over $[\theta_{I,0}-\triangle\theta,\theta_{I,0}+\triangle\theta]$ under a level η is

$$\begin{aligned} \min_{\boldsymbol{w}} \quad & F(\boldsymbol{w})=\left\|\boldsymbol{X}^H\boldsymbol{w}\right\|_p^p \qquad (p>2) \\ \text{s.t.} \quad & \boldsymbol{w}^H\boldsymbol{\alpha}(\theta_0)=1 \\ & \boldsymbol{w}^H\boldsymbol{Q}_{\text{sub}}\boldsymbol{w}\le\eta, \end{aligned} \tag{9}$$

where $\boldsymbol{Q}_{\text{sub}}=1/(2\triangle\theta)\int_{\theta_{I,0}-\triangle\theta}^{\theta_{I,0}+\triangle\theta}\boldsymbol{\alpha}(\triangle\theta_I)\boldsymbol{\alpha}^H(\triangle\theta_I)d\triangle\theta_I$ with $\boldsymbol{Q}_{\text{sub}}$ being a Hermitian matrix, and η is the predefined level of the null sector. Moreover, the average power of the MDDR beamformer over the sector $[\theta_{I,0}-\triangle\theta,\theta_{I,0}+\triangle\theta]$ can be expressed as

$$\boldsymbol{P}(\triangle\theta_I)=\frac{1}{2\triangle\theta}\int_{\theta_{I,0}-\triangle\theta}^{\theta_{I,0}+\triangle\theta}\mathrm{E}\left\{\left|\boldsymbol{w}^H\boldsymbol{\alpha}(\triangle\theta_I)\right|^2\right\}d\triangle\theta_I. \tag{10}$$

Applying eigendecomposition to $\boldsymbol{Q}_{\text{sub}}$, one has $\boldsymbol{Q}_{\text{sub}}=\boldsymbol{V}\Lambda\boldsymbol{V}^H$, where $\boldsymbol{V}=[\boldsymbol{v}_1,\cdots,\boldsymbol{v}_M]$ with $\boldsymbol{v}_m\in\mathbb{C}^M$ for $m=1,2,\cdots,M$ being the orthogonal eigenvector, and $\Lambda=\mathrm{diag}(\lambda_1,\cdots,\lambda_M)$ with diagonal elements in descending order. Assume that the rank of $\boldsymbol{Q}_{\text{sub}}$ is $r\le M$, $\boldsymbol{V}_r=[\boldsymbol{v}_1,\cdots,\boldsymbol{v}_r]$ is an orthonormal basis for the range space of matrix $\boldsymbol{Q}_{\text{sub}}$ denoted as $R(\boldsymbol{Q}_{\text{sub}})$, and the other orthogonal eigenvectors constitute its null-space $N(\boldsymbol{Q}_{\text{sub}})$.

To achieve a deeper null sector against strong fast-moving interferences, the value of η is preferred to be zero, which leads to the quadratic constraint denoted in (9) that is equivalent to a linear constraint $\boldsymbol{w}^H\boldsymbol{V}_r=\boldsymbol{0}_{r\times1}^T$, i.e., the weight vector $\boldsymbol{w}$ lies in the null-space $N(\boldsymbol{Q}_{\text{sub}})$. Furthermore, the two linear constraints are combined as

$$\widehat{\boldsymbol{V}}^H\boldsymbol{w}=\boldsymbol{e}_1, \tag{11}$$

where $\widehat{\boldsymbol{V}}=[\boldsymbol{\alpha}(\theta_0),\boldsymbol{V}_r]$, ${\boldsymbol{e}_1}^T=[1,\boldsymbol{0}_{r\times1}^T]$.

Therefore, the optimization problem in (9) with the updated linear constraint is rewritten as

$$\begin{aligned} \min_{\boldsymbol{w}} \quad & F(\boldsymbol{w})=\left\|\boldsymbol{X}^H\boldsymbol{w}\right\|_p^p \qquad (p>2) \\ \text{s.t.} \quad & \widehat{\boldsymbol{V}}^H\boldsymbol{w}=\boldsymbol{e}_1. \end{aligned} \tag{12}$$

The optimization problem shown in (12) with a linear constraint can be solved more efficiently than the one in (9). Moreover, the null depth achieved by (12) is deeper than that achieved by (9), as the quadratic constraint is set to zero.

3.1.2. Choice of p

The MDDR beamformer implicitly exploits the non-Gaussianity of signals, which significantly improves the performance of non-Gaussian signal reception. However, there is no explicit formula to describe the relationship between p and κ_s [24–26]. The general guideline is that p is determined by the non-Gaussianity of signals indicated by κ_s, that is, $p>2$ for sub-Gaussian signals and $p<2$ for super-Gaussian signals. Particularly, for sub-Gaussian signals the larger value of p leads to better performance in terms of output SINR. The near-optimal performance is achieved when $p\to\infty$ [25]. However, too large value of p is easy to result in overflow when calculating the pth power of a number in engineering application. Fortunately, for sub-Gaussian signals, such as PSK and QAM, the performance of MDDR beamformer is satisfied when the value of p is around 20 [26].

3.2. GP Algorithm

For the optimization problem in (12), the objective function and constraint are both convex, while the variable is a complex vector. Conventional methods for solving the convex optimization problem can be modified to solve this problem. In the following subsections, an efficient algorithm is developed for solving this minimization problem following the framework of GP algorithm.

3.2.1. Projection onto the feasible region

The feasible region of (12) is denoted as $\mathcal{C}=\left\{\boldsymbol{w}|\widehat{\boldsymbol{V}}^H\boldsymbol{w}=\boldsymbol{e}_1\right\}$. For any vector $\boldsymbol{s}$ not belonging to $\mathcal{C}$, the projection of $\boldsymbol{s}$ onto $\mathcal{C}$ is indicated as $P_{\mathcal{C}}(\cdot)$, which is the point located at $\mathcal{C}$ with the shortest distance to $\boldsymbol{s}$. The problem of searching for $P_{\mathcal{C}}(\boldsymbol{s})$ can be expressed as

$$\begin{aligned} \min_{\boldsymbol{w}} \quad & \|\boldsymbol{w}-\boldsymbol{s}\|^2 \\ \text{s.t.} \quad & \widehat{\boldsymbol{V}}^H\boldsymbol{w}=\boldsymbol{e}_1. \end{aligned} \tag{13}$$

Applying the method of Lagrange multipliers, we have:

$$L(\boldsymbol{w},\boldsymbol{\lambda})=\|\boldsymbol{w}-\boldsymbol{s}\|^2+\left(\boldsymbol{w}^H\widehat{\boldsymbol{V}}-\boldsymbol{e}_1^T\right)\boldsymbol{\lambda}, \tag{14}$$

where $\boldsymbol{\lambda}\in\mathbb{C}^{r+1}$. Taking the derivative w.r.t. $\boldsymbol{w}$ and setting the resultant expression to zero yield

$$\boldsymbol{w}=\boldsymbol{s}-\widehat{\boldsymbol{V}}\boldsymbol{\lambda}. \tag{15}$$

Substituting (15) into $\widehat{\boldsymbol{V}}^H\boldsymbol{w}=\boldsymbol{e}_1$ leads to

$$\boldsymbol{\lambda}=\left(\widehat{\boldsymbol{V}}^H\widehat{\boldsymbol{V}}\right)^{-1}\left(\widehat{\boldsymbol{V}}^H\boldsymbol{s}-\boldsymbol{e}_1\right). \tag{16}$$

Therefore, substitute (16) into (15) yields

$$\boldsymbol{w}=\boldsymbol{s}-\widehat{\boldsymbol{V}}\left(\widehat{\boldsymbol{V}}^H\widehat{\boldsymbol{V}}\right)^{-1}\left(\widehat{\boldsymbol{V}}^H\boldsymbol{s}-\boldsymbol{e}_1\right). \tag{17}$$

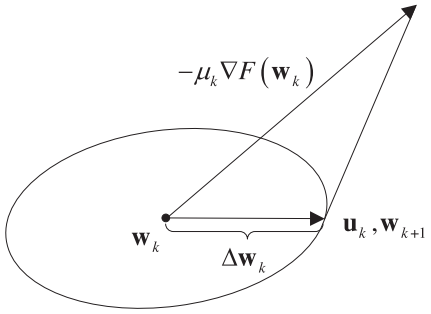

Fig. 1. Geometrical interpretation of GP algorithm.

3.2.2. GP Algorithm

The geometrical interpretation of the GP algorithm is shown in Fig. 1. Take the kth iteration as an example to elaborate the GP algorithm. First, the gradient of $F(\boldsymbol{w}_k)$ is calculated at point $\boldsymbol{w}_k$ (with details given in Appendix). Second, the step size μ_k along the direction of gradient descent is determined. Then, projecting $F(\boldsymbol{w}_k) - \mu_k \nabla F(\boldsymbol{w}_k)$ onto the feasible region $\mathcal{C}$ with $\boldsymbol{u}_k = P_{\mathcal{C}}(F(\boldsymbol{w}_k) - \mu_k \nabla F(\boldsymbol{w}_k))$, the updated direction is $\triangle \boldsymbol{w}_k = \boldsymbol{u}_k - \boldsymbol{w}_k$. Finally, $\boldsymbol{w}_{k+1}$ is given by following the direction $\triangle \boldsymbol{w}_k$ with step size α_k, i.e., $\boldsymbol{w}_{k+1} = \boldsymbol{w}_k + \alpha_k \triangle \boldsymbol{w}_k$. Setting $\alpha_k = 1$, one has $\boldsymbol{w}_{k+1} = \boldsymbol{u}_k$.

The last problem to determine the step size μ_k along the direction of $-\nabla F(\boldsymbol{w}_k)$, which minimizes the objective function $F(\boldsymbol{w})$. The minimization problem can be formulated as

$$\mu_k = \arg\min_{\mu>0} F(P_{\mathcal{C}}(\boldsymbol{w}_k - \mu \nabla F(\boldsymbol{w}_k))). \tag{18}$$

Then, the backtracking line search algorithm is utilized to provide the optimal μ_k [31], which, when adopted, leads to the GP algorithm and is summarized as Algorithm 1.

Algorithm 1 GP Algorithm.

Input:
Data received by array: $\boldsymbol{X}$
Maximum iteration number: $K_{\max}$
Convergence tolerance: ε
Initialize:
$\boldsymbol{w}_0 = \boldsymbol{\alpha}(\theta_0)/\|\boldsymbol{\alpha}(\theta_0)\|^2$
$\widehat{\boldsymbol{V}} = [\boldsymbol{\alpha}(\theta_0), \boldsymbol{V}_r]$
$\alpha_k = 1$
$\mu_0 = 1$
$\gamma = 0.5$
$\delta = 0.1$
for $k = 0, 1, \cdots, K_{\max}$ **do**
  Compute $\boldsymbol{u}_k = P_{\mathcal{C}}(\boldsymbol{w}_k - \mu_k \nabla F(\boldsymbol{w}_k))$
    $\triangle \boldsymbol{w}_k = \boldsymbol{u}_k - \boldsymbol{w}_k$
    for $i = 1, 2, \cdots$ **do**
    Compute $\boldsymbol{w}_{k+1} = P_{\mathcal{C}}(\boldsymbol{w}_k - \mu \nabla F(\boldsymbol{w}_k))$
      Break if $F(\boldsymbol{w}_{k+1}) < F(\boldsymbol{w}_k) + \delta \cdot 2\mathrm{Re}\left(\nabla F(\boldsymbol{w}_k)^H (\boldsymbol{w}_{k+1} - \boldsymbol{w}_k)\right)$
      $\mu \leftarrow \gamma \mu$
    end for
    return $\mu_k = \mu$
  $\boldsymbol{w}_{k+1} = \boldsymbol{w}_k + \mu_k \triangle \boldsymbol{w}_k$
  Break if $\|\boldsymbol{w}_{k+1} - \boldsymbol{w}_k\| < \varepsilon$ or $k > K_{\max}$
end for
return $\boldsymbol{w}_{\text{opt}}$

The dominant computational cost for the GP algorithm is the calculation of the gradient of the objective function $F(\boldsymbol{w})$, which has a computational complexity of $\mathcal{O}(NM)$.

Table 1
Null depths provided by standard MDDR beamformer at the AOAs of 30° and 75° respectively (in dB).

p	1	1.5	2	4	8	20
30°	−20.12	−20.13	−20.09	−20.11	−20.12	−20.20
75°	−23.39	−23.44	−23.26	−23.37	−23.43	−23.89

4. Numerical results

In this section, four numerical experiments are conducted to demonstrate the performance of the optimal weight vectors achieved by the developed algorithm. As QPSK signals are typical sub-Gaussian signals which have been widely used in various areas, such as TV, WiFi and wireless communications. According to the definition of kurtosis in (6), it is easy to attain $\kappa_{\text{QPSK}} = 1$. In the following simulations, we assume that the signals of the SOI and interferences are QPSK modulated, while the noise is additive white Gaussian noise (AWGN). A ULA of 20 sensors with a half wavelength spacing is utilized. Suppose that there are four uncorrelated QPSK signal sources, distributed in the far-field of the array. The AOA of SOI is $\theta_0 = 43°$, and the AOAs of three interferences are $\theta_1 = 30°$, $\theta_2 = 75°$, and $\theta_3 = -60°$. The interference from the direction of $-60°$ is the fast-moving interference, whose width of dynamic AOA is $\triangle\theta_I = 10°$ from $-65°$ to $-55°$. Whereas the other two interferences are fixed at the AOAs of 30° and 75°. The signal-to-noise ratio (SNR) is defined as

$$\text{SNR} = \frac{\sigma_s^2}{\sigma_e^2}. \tag{19}$$

Furthermore, we assume that three interferences are stronger than the SOI, with the variances being $\sigma_1^2 = 4\sigma_s^2$, $\sigma_2^2 = 9\sigma_s^2$, and $\sigma_3^2 = 100\sigma_s^2$.

4.1. Experiment 1

In this subsection, the beampatterns for various p of the proposed approach is evaluated when SNR = 0 dB and the number of snapshots is 400. Although the MDDR beamformer is prefer to adopt $p > 2$ for sub-Gaussian signals, the scenarios of $p = 1$ and $p = 1.5$ are also involved to explore the performances of the standard MDDR and the proposed beamformer with different p. In comparison with the proposed beamformer, the beampatterns generated by the standard MDDR beamformer in the presence of fast-moving interference is shown in Fig. 2, while the simulation results of GP algorithm under the same simulation conditions are depicted in Fig. 3, in which the red dash lines indicate the pre-specified null sector and the AOA of SOI. From Figs. 2 and 3, it can be seen that the GP algorithm is able to provide a deep null of more than −80 dB over the pre-specified sector of $[-65°, -55°]$, which can suppress the strong fast-moving interferences efficiently.

Moreover, the scenario of $p = 2$ shown in Fig. 3 is the same as the one proposed in [19]. Compared with the simulation results in [19], the null depth achieved by (12) is deeper, in which the constraint on the average power over the predefined angular sector is set to zero.

Furthermore, the null depths provided by the standard MDDR beamformer and GP algorithm at the AOAs of 30° and 75° are shown in Tables 1 and 2, respectively. It can be seen that the GP algorithm provides much deeper nulls for those fixed interferences over the standard MDDR beamformer. In Table 2, deeper nulls can be achieved when the value of p is greater than 2. Recall that when $p = 2$, the MDDR beamformer is reduced to the MPDR beamformer.

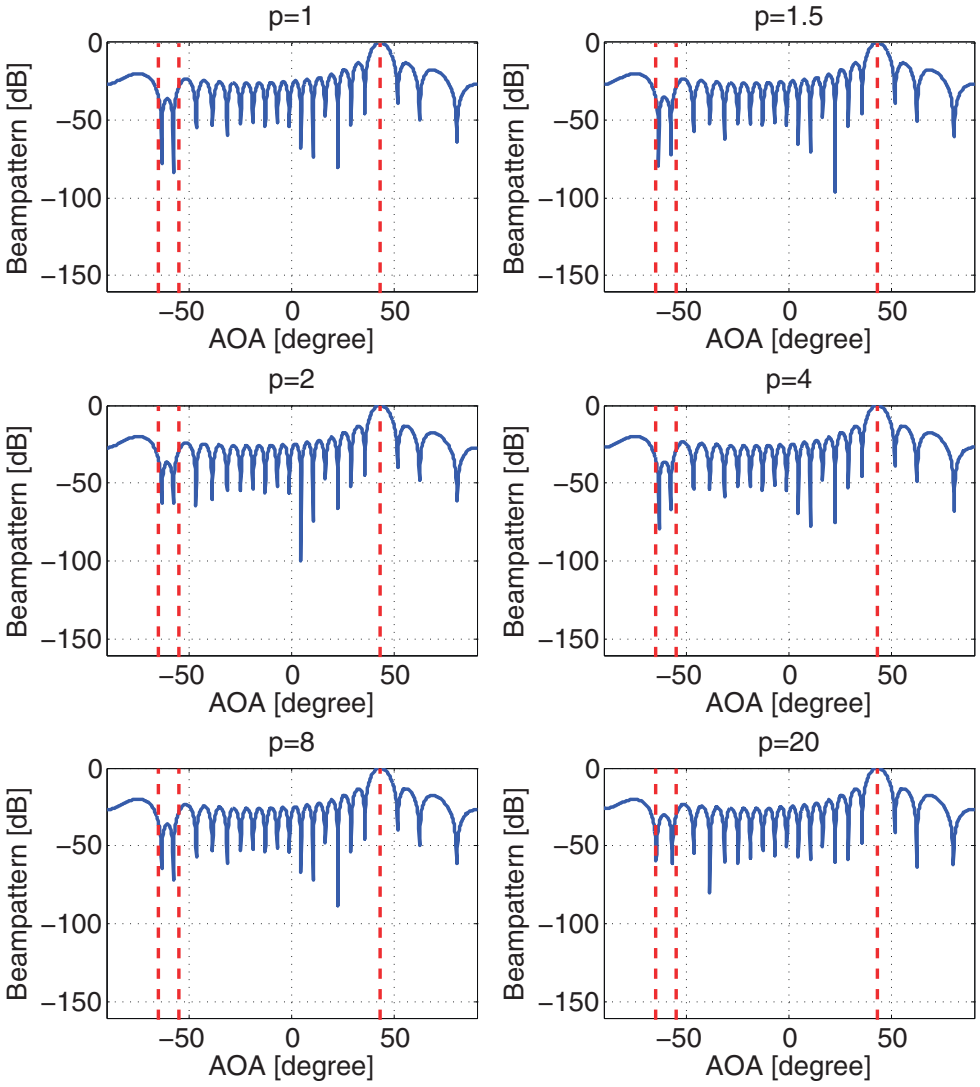

Fig. 2. Beampatterns of standard MDDR beamformer in the presence of fast-moving interference for $p = 1, 1.5, 2, 4, 8$ and 20.

Table 2
Null depths provided by GP algorithm at the AOAs of 30° and 75° respectively (in dB).

p	1	1.5	2	4	8	20
30°	−44.36	−48.20	−51.17	−58.08	−63.61	−69.40
75°	−49.12	−52.90	−54.83	−60.19	−63.83	−70.36

4.2. Experiment 2

Under the same settings as those in Experiment 1, the output SINR versus SNR with $N = 100$ is shown in Fig. 4. 200 independent trials have been conducted and the upper bound SINR is $\lambda_{\max}\left(\sigma_s^2 \boldsymbol{R}_{i+n}^{-1} \boldsymbol{\alpha}(\theta_0)\boldsymbol{\alpha}(\theta_0)^H\right)$.

It can be seen from Fig. 4 that the performance of the proposed beamformer is affected by the value of p. Specifically, the output SINR increases with the increase of p. When $p = 20$, the output SINR of the proposed beamformer is close to the upper bound, which is the reason why the larger value of p is not adopted. Comparing the experimental results of $p = 2$ and $p = 20$, it is indicated again that the MDDR beamformer exhibits better performance in sub-Gaussian signals reception than the MVDR beamformer.

4.3. Experiment 3

The output SINR versus the number of snapshots with SNR = 10 dB is shown in Fig. 5. It is seen that the output SINR increases as the number of snapshots increases. The GP algorithm is sensitive to the number of snapshots when $p \leq 8$, while the near-optimal output SINR is achieved when $p = 20$ which just needs 100 snapshots.

The proposed GP algorithm is integrated with backtracking line search algorithm to determine the optimal step size μ_k shown in (18). Exploring Algorithm 1, the value of μ_k is affected by γ and δ, which makes the algorithm converge to different $\boldsymbol{w}_{\text{opt}}$ and different output SINRs. The proposed GP algorithm is sensitive to the settings of γ and δ when p adopts small values, specially $p = 1$. The results shown in Fig. 5 are attained when $\gamma = 0.6$ and $\delta = 0.05$.

4.4. Experiment 4

In this subsection, we investigate the runtimes of the GP algorithm for $p = 4$, $p = 8$, and $p = 20$, meanwhile the experimental results of the standard convex optimization package are provided. The parameter settings are: SNR = 10 dB, $M = 20$, $\varepsilon = 0.001$, $K_{\max} = 1000$, and other parameters are listed in Algorithm 1;

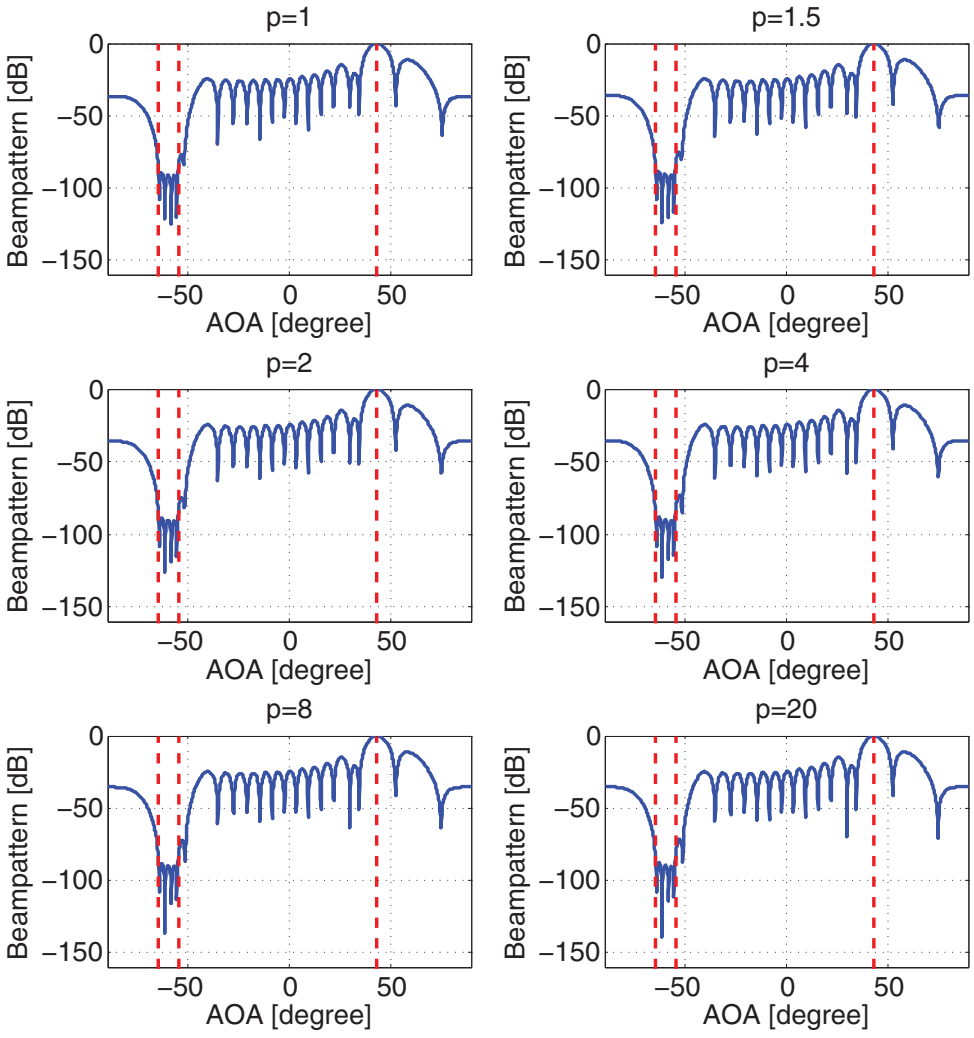

Fig. 3. Beampatterns of GP algorithm in the presence of fast-moving interference for $p = 1, 1.5, 2, 4, 8$ and 20.

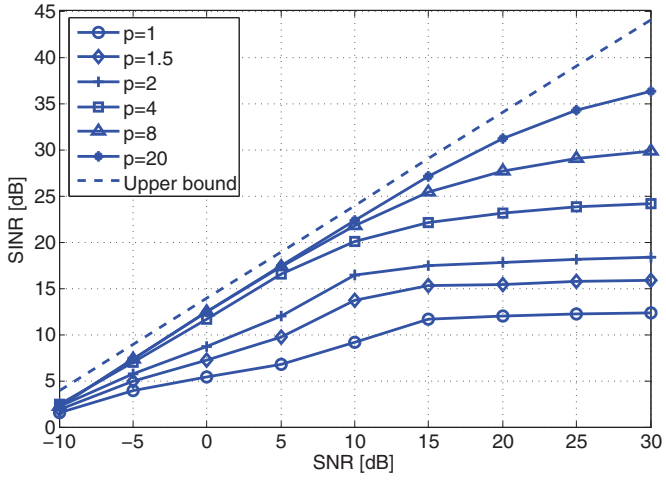

Fig. 4. Output SINR versus SNR of GP algorithm.

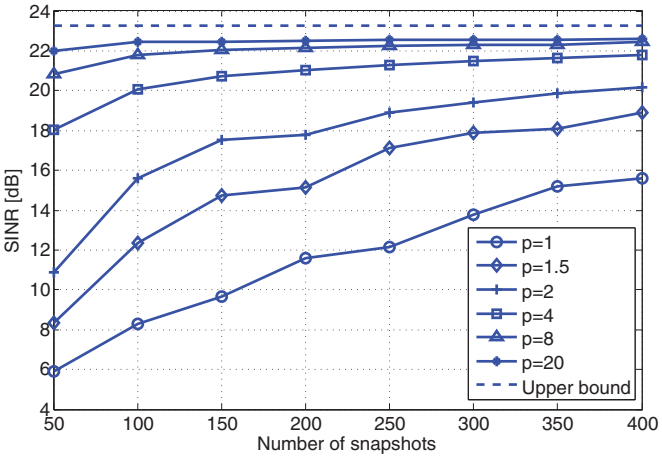

Fig. 5. Output SINR versus number of snapshots for GP algorithm.

the number of snapshots for the GP algorithm varies from 100 to 10000, while it is interrupted for CVX package at $N = 5000$ as overflow occurs; the number of independent trials is 200; other parameters not mentioned herein remain unchanged in Algorithm 1. The standard convex optimization package is CVX version 2.1, which is available at [32].

The experimental results are based on Matlab R2012b on a computer with a 3.4 GHz CPU and 8 GB memory, which are tabulated in Tables 3 and 4.

Table 3
Runtimes of GP algorithm for $p = 4, 8, 20$ (in seconds).

N	100	500	1000	5000	10000
$p = 4$	0.0060	0.0321	0.0762	0.6852	2.3657
$p = 8$	0.0072	0.0327	0.0785	0.7245	2.5766
$p = 20$	0.0084	0.0265	0.0600	0.6493	2.2581

Table 4
Runtimes of CVX for $p = 4, 8, 20$ (in seconds).

N	100	500	1000	5000
$p = 4$	1.3208	5.5706	13.3432	Out of memory
$p = 8$	1.4727	6.9229	17.0201	Out of memory
$p = 20$	2.3510	11.7799	26.4071	Out of memory

The IPM based CVX package has the computational complexity of $\mathcal{O}(N^3)$, while that of the GP algorithm is $\mathcal{O}(NM)$. As $M \ll N$, the GP algorithm is much more efficient for the problem in (12) under the same experimental conditions. Comparing the results shown in Tables 3 and 4, the same conclusion can be drawn.

5. Conclusion

Most of signals encountered in real-world applications are non-Gaussian distributed. The MVDR beamformer and its variants, based on the minimum variance criterion, turn out to be sub-optimal for non-Gaussian signals as they just exploit the second-order statistical information of non-Gaussian signals. The MDDR approach was proposed to handle the non-Gaussianity of signals with the aim at improving the reception of non-Gaussian signals. This paper extends the MDDR beamformer to handle fast-moving interferences, in which a continuous deep null sector over a predefined range of dynamic AOA is desired. To make the MDDR beamformer robust against the fast-moving interference, the proposed beamformer minimizes the output based on the MD criterion and constrains the average power over the dynamic AOA to be zero via a quadratic constraint. In order to reduce the computational complexity, a linear rather than a quadratic constraint is derived. Furthermore, the GP algorithm is developed. Experimental results confirm that the proposed beamforming approach is able to suppress the fast-moving interferences effectively.

Acknowledgement

The authors would like to thank the reviewers for their constructive comments and helpful suggestions. This work was supported by the National Natural Science Foundation of China under Grant U1501253, the Natural Science foundation of Guangdong Province, P.R. China (No.2015A030311030), the Foundation of Shenzhen City under Grants ZDSYS201507081625213 and JCYJ20160520165659418, the Foundation of Nanshan District Shenzhen City under Grant KC2015ZDYF0036 and the China Postdoctoral Science Foundation under Grant 2017M610547.

Appendix

Consider the conversion of the objective function of (12) into the expression of ℓ_2-norm, that is,

$$F(\boldsymbol{w}) = \left\|\boldsymbol{X}^H\boldsymbol{w}\right\|_p^p = \sum_{n=1}^{N}\left|\boldsymbol{x}^H(n)\boldsymbol{w}\right|^{p-2}\left|\boldsymbol{x}(n)^H\boldsymbol{w}\right|^2. \tag{20}$$

Since $\boldsymbol{y} = \boldsymbol{X}^H\boldsymbol{w}$, the objective function can be rewritten as

$$\begin{aligned} F(\boldsymbol{w}) &= \left\| \begin{bmatrix} |\boldsymbol{y}(1)|^{\frac{p-2}{2}} & \cdots & 0 \\ \vdots & \ddots & \vdots \\ 0 & \cdots & |\boldsymbol{y}(N)|^{\frac{p-2}{2}} \end{bmatrix} \begin{bmatrix} |\boldsymbol{y}(1)| \\ \vdots \\ |\boldsymbol{y}(N)| \end{bmatrix} \right\|^2 \\ &= \|\boldsymbol{\Sigma}\boldsymbol{y}\|^2 \\ &= \boldsymbol{y}^H\boldsymbol{\Sigma}^H\boldsymbol{\Sigma}\boldsymbol{y} \\ &= \boldsymbol{w}^H\boldsymbol{X}\boldsymbol{C}(\boldsymbol{w})\boldsymbol{X}^H\boldsymbol{w} \\ &= \boldsymbol{w}^H\widetilde{\boldsymbol{R}}(\boldsymbol{w})\boldsymbol{w}, \end{aligned} \tag{21}$$

where $\boldsymbol{\Sigma} = \mathrm{diag}\left\{|y(1)|^{(p-2)/2}, \cdots, |y(N)|^{(p-2)/2}\right\}$. Note that $\boldsymbol{C}(\boldsymbol{w}) = \boldsymbol{\Sigma}^H\boldsymbol{\Sigma}$ and $\widetilde{\boldsymbol{R}}(\boldsymbol{w}) = \boldsymbol{X}\boldsymbol{C}(\boldsymbol{w})\boldsymbol{X}^H$ are the functions of $\boldsymbol{w}$.

If g is a real function of a complex vector $\boldsymbol{z}$, then the complex gradient vector is given by [33]

$$\nabla g(\boldsymbol{z}) = 2\frac{dg(\boldsymbol{z})}{d\boldsymbol{z}^*} = \frac{\partial g(\boldsymbol{z})}{\partial \mathrm{Re}(\boldsymbol{z})} + i\frac{\partial g(\boldsymbol{z})}{\partial \mathrm{Im}(\boldsymbol{z})}. \tag{22}$$

As a result, the gradient of $F(\boldsymbol{w})$ w.r.t. the complex vector $\boldsymbol{w}$ is expressed as

$$\nabla F(\boldsymbol{w}) = \frac{p}{2}\boldsymbol{X}\boldsymbol{C}(\boldsymbol{w})\boldsymbol{X}^H\boldsymbol{w}. \tag{23}$$

References

[1] J. Li, P. Stoica, Robust Adaptive Beamforming, Wiley Online Library, 2006.
[2] L.C. Godara, Application of antenna arrays to mobile communications. II. Beam-forming and direction-of-arrival considerations, Proc. IEEE 85 (8) (1997) 1195–1245.
[3] J. Yin, Underwater acoustic communications and signal processing, National Defense Industry Press, 2011.
[4] S.A. Vorobyov, Principles of minimum variance robust adaptive beamforming design, Signal Process. 93 (12) (2013) 3264–3277.
[5] Q. Li, B. Liao, L. Huang, C. T. Guo, G. S. Liao, S. Q. Zhu, A robust stap method for airborne radar with array steering vector mismatch, Signal Process. 128 (2016) 198–203.
[6] B.D. Carlson, Covariance matrix estimation errors and diagonal loading in adaptive arrays, IEEE Trans. Aerosp. Electron.Syst. 24 (4) (1988) 397–401.
[7] C.Y. Chen, P.P. Vaidyanathan, Quadratically constrained beamforming robust against direction-of-arrival mismatch, IEEE Trans. Signal Process. 55 (8) (2007) 4139–4150.
[8] J. Li, P. Stoica, Z. Wang, On robust Capon beamforming and diagonal loading, IEEE Trans. Signal Process. 51 (7) (2003) 1702–1715.
[9] R.G. Lorenz, S.P. Boyd, Robust minimum variance beamforming, IEEE Trans. Signal Process. 53 (5) (2005) 1684–1696.
[10] L. Zhang, B. Liao, L. Huang, C. Guo, An eigendecomposition-based approach to blind beamforming in a multipath environment, IEEE Communications Letters 21 (2) (2017) 322–325.
[11] S. Shahbazpanahi, A.B. Gershman, Z.-Q. Luo, K.M. Wong, Robust adaptive beamforming for general-rank signal models, IEEE Trans. Signal Process. 51 (9) (2003) 2257–2269.
[12] S.A. Vorobyov, A.B. Gershman, Z.-Q. Luo, Robust adaptive beamforming using worst-case performance optimization: a solution to the signal mismatch problem, IEEE Trans. Signal Process. 51 (2) (2003) 313–324.
[13] H.L. Van Trees, Detection, Estimation, and Modulation Theory, Part IV: Optimum Array Processing, Wiley-Interscience, 2002.
[14] R.J. Mailloux, Covariance matrix augmentation to produce adaptive array pattern troughs, Electron. Lett. 31 (10) (1995) 771–772.
[15] M. Zatman, Production of adaptive array troughs by dispersion synthesis, Electron. Lett. 31 (25) (1995) 2141–2142.
[16] A.B. Gershman, U. Nickel, J.F. Bohme, Adaptive beamforming algorithms with robustness against jammer motion, IEEE Trans. Signal Process. 45 (7) (1997) 1878–1885.
[17] A.B. Gershman, G.V. Serebryakov, J.F. Bohme, Constrained hung-turner adaptive beam-forming algorithm with additional robustness to wideband and moving jammers, IEEE Trans. Antennas Propag. 44 (3) (1996) 361–367.
[18] J. Riba, J. Goldberg, G. Vazquez, Robust beamforming for interference rejection in mobile communications, IEEE Trans. Signal Process. 45 (1) (1997) 271–275.
[19] A. Amar, M.A. Doron, A linearly constrained minimum variance beamformer with a pre-specified suppression level over a pre-defined broad null sector, Signal Process. 109 (2015) 165–171.
[20] H. Mathis, On the kurtosis of digitally modulated signals with timing offsets, in: Proc. 2001 IEEE Third Workshop on Signal Processing Advances in Wireless Communications, 2001, pp. 86–89.
[21] D. Middleton, Non-Gaussian noise models in signal processing for telecommunications: new methods an results for class A and class B noise models, IEEE Trans. Inf. Theory 45 (4) (1999) 1129–1149.

[22] J.F. Cardoso, A. Souloumiac, Blind beamforming for non-Gaussian signals, IEE Proc. F - Radar Signal Process. 140 (6) (1993) 362–370.
[23] P. Tsakalides, C.L. Nikias, Robust adaptive beamforming in alpha-stable noise environments, in: Proc. 1996 IEEE International Conference on Acoustics, Speech, and Signal Processing Conference Proceedings, 1996, pp. 2884–2887.
[24] X. Jiang, W.J. Zeng, A. Yasotharan, H.C. So, T. Kirubarajan, Minimum dispersion beamforming for non-Gaussian signals, IEEE Trans. Signal Process. 62 (7) (2014a) 1879–1893.
[25] X. Jiang, W.J. Zeng, A. Yasotharan, H.C. So, T. Kirubarajan, Robust beamforming by linear programming, IEEE Trans. Signal Process. 62 (7) (2014b) 1834–1849.
[26] X. Jiang, W.J. Zeng, A. Yasotharan, H.C. So, T. Kirubarajan, Quadratically constrained minimum dispersion beamforming via gradient projection, IEEE Trans. Signal Process. 63 (1) (2015) 192–205.
[27] X. Jiang, W.J. Zeng, H.C. So, A.M. Zoubir, T. Kirubarajan, Beamforming via nonconvex linear regression, IEEE Trans. Signal Process. 64 (7) (2016) 1714–1728.
[28] S. Boyd, L. Vandenberghe, Convex Optimization, Cambridge University Press, 2004.
[29] A.M. Zoubir, V. Koivunen, Y. Chakhchoukh, M. Muma, Robust estimation in signal processing: a tutorial-style treatment of fundamental concepts, IEEE Signal Process. Mag. 29 (4) (2012) 61–80.
[30] S. Gazor, W. Zhang, Speech probability distribution, IEEE Signal Process. Lett. 10 (7) (2003) 204–207.
[31] A. Antoniou, W.-S. Lu, Practical Optimization: Algorithms and Engineering Applications, Springer Science & Business Media, 2007.
[32] M. Grant, S. Boyd, CVX: Matlab Software for Disciplined Convex Programming, Version 2.1, 2014. (http://cvxr.com/cvx).
[33] S. Haykin, Adaptive Filter Theory, Prentice Hall, 2002.